JACS
JOURNAL OF THE AMERICAN CHEMICAL SOCIETY
Communication
pubs.acs.org/JACS

High-Efficiency Solution-Processed $Cu_2ZnSn(S,Se)_4$ Thin-Film Solar Cells Prepared from Binary and Ternary Nanoparticles

Yanyan Cao,* Michael S. Denny, Jr., Jonathan V. Caspar, William E. Farneth, Qijie Guo, Alex S. Ionkin, Lynda K. Johnson, Meijun Lu, Irina Malajovich, Daniela Radu, H. David Rosenfeld, Kaushik Roy Choudhury, and Wei Wu

DuPont Central Research and Development, Experimental Station, Wilmington, Delaware 19880, United States

Supporting Information

ABSTRACT: A new solution-based method to fabricate $Cu_2ZnSn(S,Se)_4$ (CZTSSe) thin films is presented. Binary and ternary chalcogenide nanoparticles were synthesized and used as precursors to form CZTSSe thin films. The composition of the CZTSSe films can be easily controlled by adjusting the ratio of the nanoparticles used. The effect of compositional adjustment on device performance is illustrated. Laboratory-scale photovoltaic cells with 8.5% total-area efficiency (or 9.6% active-area efficiency) were demonstrated without anti-reflective coatings. Material characterization data revealed the formation of a bilayer microstructure during thermal processing and suggested a path forward on device improvement.

Current high-efficiency absorber layers in thin-film photovoltaic (PV) cells, such as copper indium gallium sulfide/selenide (CIGS) and cadmium telluride (CdTe), rely upon low-abundance elements and thus are predicted to face supply shortages in the long run.[1] In response to this forecast, interest in Cu_2ZnSnS_4 (CZTS) and $Cu_2ZnSn(S,Se)_4$ (CZTSSe) as sustainable alternatives to CIGS has been rapidly increasing.[2] In addition to their earth-abundant compositions, CZTS and CZTSSe offer the promise of PV performance similar to that of CIGS,[3] since they are iso-structural, have a near-ideal band gap energy for a single-junction PV device (1.5 eV, CZTS) with tunability from about 1.0 to 1.5 eV by adjustment of the Se/S ratio in CZTSSe and a high optical absorption coefficient ($\sim 10^4$ cm^{-1}).[4,5] The opportunity to build upon the substantial body of knowledge developed for CIGS is also expected to hasten improvements in CZTS and CZTSSe PV devices.

Various methods have been developed to fabricate CZTS and CZTSSe thin films suitable for solar cell applications. Several high-vacuum deposition techniques have been employed to prepare CZTS films. The pioneering work of Katagiri's group demonstrated 6.7% efficiency CZTS solar cells fabricated by sulfurizing a co-sputtered precursor layer consisting of metals and/or metal chalcogenides.[6] Thermal evaporation[7,8] and E-beam evaporation[9] have also been used to deposit CZTS precursor films. CZTS has been formed in a single step through co-evaporation,[10,11] reactive sputtering,[12] or pulsed laser deposition.[13] However, these high-vacuum deposition techniques generally require complex equipments and are consequently costly to implement on large scale. In contrast, solution-based deposition routes could potentially provide low-cost scalable routes to CZTS and CZTSSe devices. Several such solution routes have been reported, including electroplating,[14] sol–gel coating,[15] spray pyrolysis,[16] and chemical bath deposition.[17] Especially noteworthy is the fabrication of CZTS films from quaternary CZTS nanocrystals,[18−21] where the use of nanoparticle inks simplified processing. Thermal annealing in the presence of selenium yielded CZTSSe PV devices with 7.2% efficiency.[22] However, it has been shown that the performance of CZTS devices is strongly influenced by the specific CZTS composition (especially by the Cu/Zn/Sn ratios),[23] and the quaternary nanoparticle-based synthetic routes do not offer a simple method by which the final film composition can be controlled.[21] Recently Mitzi et al.[24] reported a solution-based route to CZTSSe, which offers improved control over composition and has yielded a record device efficiency of 10.1%.[25] While the improvement in performance is impressive, it comes at the expense of using hydrazine as the coating solvent, which is both highly toxic and potentially explosive. Our group[26] and others[27] have been working on solution processes that rely on safer precursor chemistries. Here we report our results with a synthesis approach based on binary and ternary nanoparticles that allows facile control of film composition.

We start by synthesizing binary and ternary nanoparticle metal sulfides. The nanoparticles are then dispersed and combined in solution to yield "inks" with a particular metal composition. This approach reduces the problem of composition control to a simple mixing of precursors in known proportions. The resulting ink blends can then be cast into thin films by standard methods like spin-coating to yield smooth, dense CZTS precursor coatings, which are subsequently converted into CZTS or CZTSSe in a thermal processing step described in more detail below. We have used this method to prepare CZTSSe PV devices of 8.5% total-area efficiency without much optimization and without an anti-reflective coating.

A complete precursor set of binary and ternary sulfide nanoparticles, including copper tin sulfide (CTS), ZnS, SnS, CuS, and Cu_7S_4, was synthesized by reacting metal salts with sulfur in oleylamine and trioctylphosphine oxide (TOPO).[28] Interestingly, when $CuCl_2$ was used as the starting material,

Received: June 14, 2012
Published: September 10, 2012

   dx.doi.org/10.1021/ja3057985 | J. Am. Chem. Soc. 2012, 134, 15644−15647

CuS nanoparticles were obtained, while Cu_7S_4 nanoparticles resulted when CuCl was employed. Both CuS and Cu_7S_4 nanoparticles can be used to form CZTS films. Transmission electron microscopy (TEM) images of CTS nanoparticles and ZnS nanoparticles are shown in Figure 1. Most of the

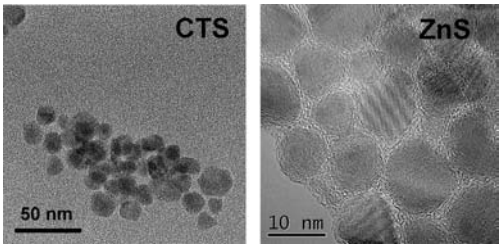

Figure 1. TEM images of the CTS and ZnS nanoparticles made.

nanoparticles are irregular in shape, with sizes varying from several nanometers to a few tens of nanometers. The detailed synthesis procedure and characterization of the nanoparticles are included in the Supporting Information. It is worth noting that the CTS nanoparticle product was actually a mixture of Cu_2SnS_3 and some binary sulfides, mainly copper sulfides according to X-ray absorption spectroscopy and inductively coupled plasma atomic emission spectroscopy (ICP-AES). Therefore, when CTS and ZnS were used as precursors, SnS nanoparticles were often used to adjust the Cu/Sn ratio in the final film.

CZTSSe thin films were prepared by combining an appropriate mixture of binary and ternary nanoparticles to form an ink, followed by annealing in the presence of selenium; two examples are shown below. In eq 1, a mixture of CTS and ZnS nanoparticles and a small amount of SnS nanoparticles are used as precursors. In eq 2, a simple mixture of binary nanoparticles is employed. Following spin-coating of the inks and thermal processing, CZTSSe is formed from both routes, as confirmed by XRD (Figures S8 and S10). While not the focus of this paper, we have also found that annealing these precursor films in either argon or sulfur-rich atmospheres yields CZTS.

$$\text{CTS} + \text{ZnS} + \text{SnS} \xrightarrow{\Delta\text{Se}} \text{CZTSSe} \quad (1)$$

$$\text{Cu}_x\text{S}_y + \text{ZnS} + \text{SnS} \xrightarrow{\Delta\text{Se}} \text{CZTSSe} \quad (2)$$

Using CZTSSe films described above, solar cells were fabricated using a device structure typical for CIGS cells (see Supporting Information for experimental details).[29] Briefly, soda lime glass (SLG) coated with 0.75 μm of Mo served as the substrate and back contact. The complete device stack was SLG/Mo/CZTSSe/CdS/i-ZnO/ITO. CdS was applied via chemical bath deposition, while i-ZnO and ITO were deposited by sputtering. Electrical connections to ITO were made via Ag contacts evaporated through a patterned shadow mask.

Figure 2 shows the current density–voltage (J–V) characteristics and the external quantum efficiency response (EQE) of a CZTSSe PV device made from binary and ternary precursors. The device exhibits a total-area efficiency of 8.5% (active-area efficiency of 9.6%) under simulated 1 sun AM 1.5 G illumination, representing one of the highest efficiencies reported to date for CZTSSe PV devices.

The EQE response (Figure 2B) yields an estimated CZTSSe band gap of 1.1 eV. This value indicates a high level (>90%) of replacement of sulfur in the precursor coatings by selenium

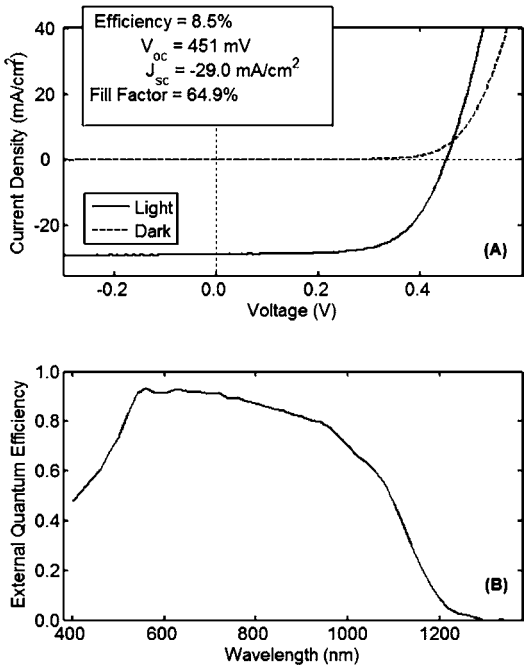

Figure 2. (A) J–V characteristics of a CZTSSe solar cell fabricated from the binary and ternary nanoparticles. Measurements were performed in the dark and under simulated 1 sun AM 1.5 G illumination at room temperature. (B) EQE of the same device.

during annealing.[30,31] This is consistent both with the relatively low value of V_{oc} observed in the J–V response and with results from XRD (Figure S10). It is also consistent with the copper edge X-ray absorption near-edge structure (XANES) data, which suggests that in a similar sample, 90% of Cu is present as CZTSe and 8% of Cu is present as CZTS.[32] Previous results[33] suggest that further improvement in device efficiency will be observed with lower levels of Se incorporation; we are actively pursuing alternative annealing strategies to test these predictions.

Scanning electron microscopy (SEM, Figure 3A) revealed a surprisingly complex internal microstructure for a similar device. The columnar bottom layer is typical of Mo. Under our current selenium-rich thermal processing conditions, an approximately 0.5 μm thick layer of $MoSe_2$ forms on top of Mo. The CZTSSe layer is seen to comprise a fine-grained sublayer and a large-grained outer layer. The collection of densely packed nanoparticles in the small-grain layer is reminiscent of the precursor film before annealing (Figure S9). The large-grain layer forms during thermal processing and consists of densely packed micrometer-sized crystals of CZTSSe.

To better understand the speciation within the device layers, we employed Auger depth profiling. Data (Figure 3B) were collected on the same device whose cross-section was shown in Figure 3A, employing sputtering with a defocused ion beam and Zalar rotation. When combined with the cross-sectional SEM data, the results demonstrate that the CZTSSe large-grain and small-grain layers have significantly different compositions. The small-grain layer, especially near the Mo interface, is rich in carbon, while the large-grain layer is shown to be nearly carbon-free. The large-grain layer is composed of high-purity crystalline CZTSSe and is likely responsible for the majority of the observed photoresponse of the PV device. Quantitative analysis of the Auger data in the large-grain region led to elemental ratios that can be summarized in this formula:

dx.doi.org/10.1021/ja3057985 | J. Am. Chem. Soc. 2012, 134, 15644–15647

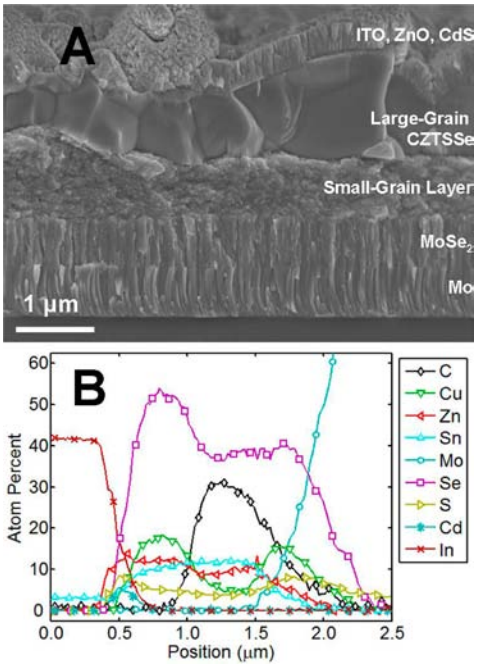

Figure 3. (A) Cross-sectional SEM image and (B) Auger depth profile of a finished CZTSSe solar cell.

$Cu_{1.7}Zn_{1.2}SnS_{0.6}Se_{5.0}$. High-resolution TEM (not shown) reveals the small-grain layer as consisting of CZTSSe nanoparticles as well as binary/ternary chalcogenide precursor nanoparticles embedded in an amorphous matrix containing a significant amount of carbon. We speculate the high carbon content helps to make the small-grain layer electrically conductive. Series resistance resulting from the combination of the small-grain layer and the back surface $MoSe_2$ layer very likely has an adverse impact on the PV device performance. Management of the carbon content in our inks as well as $MoSe_2$ formation will likely lead to further device improvement.[7,34]

A key advantage of the synthetic approach reported here is the direct and easy control of the ratios of the three metals in the final CZTSSe films. In order to demonstrate this for the route described in eq 1, dispersions of CTS, ZnS, and SnS nanoparticles were combined in different ratios to form a series of inks. These inks were cast onto Mo-coated SLG substrates and converted to CZTSSe through simultaneous annealing. The overall metal ratios in the final annealed films, as determined by ICP-AES, were shown to depend systematically on the volume ratios of the precursor inks (Figure S6).

The importance of stoichiometry control given the prominent effect of composition on device performance is illustrated in Figure 4. Samples 1 and 2 differ only in the precursor ink ratios used; all other conditions were kept identical during the cell buildup. According to XRD, CZTSSe is the dominant phase for both samples, although we cannot exclude the possibility of the existence of some secondary phases and amorphous impurities. However, their device performance differs significantly as a result of the different elemental ratios. Sample 1 has higher total-area efficiency (6.0% vs 2.0% in sample 2) as a result of improved fill factor (FF), short-circuit current density (J_{sc}), and slightly better open-circuit voltage (V_{oc}). According to ICP-AES, sample 1 is copper-poor and zinc-rich (Cu/Sn = 1.64, Zn/Sn = 1.17), while sample 2 is close to the $Cu_2ZnSn(S,Se)_4$ formula stoichiometry

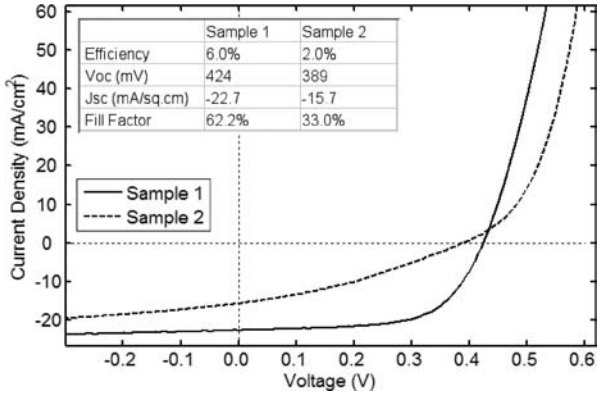

Figure 4. *J*–*V* characteristics of two CZTSSe PV cells under illumination.

(Cu/Sn = 1.96, Zn/Sn = 1.08). Although there is some agreement in the literature that copper-poor and zinc-rich films tend to have higher efficiencies,[23] there is no consensus on the exact optimal stoichiometry. The reason why stoichiometry plays such an important role is not well understood, either. The method reported in this paper has created a convenient model system to study the effect of elemental ratios in the CZTSSe film on the resulting solar cells as well as to help the mechanistic understanding of this effect.

In conclusion, a new method to fabricate CZTS and CZTSSe thin films has been developed that allows facile control of metal ratios in the resulting films. Binary and ternary sulfide nanoparticles were used to generate a dense and smooth precursor layer, which was then converted to CZTSSe via annealing in the presence of selenium. CZTSSe PV devices with total-area efficiencies of 8.5% have been demonstrated. Metal ratio and S/Se ratio optimization, control over bilayer formation, and reduction of the back contact selenization remain focus areas for device improvement.

■ ASSOCIATED CONTENT

Ⓢ Supporting Information

Experimental details on nanoparticle synthesis, solar cell fabrication, and characterization. This material is available free of charge via the Internet at http://pubs.acs.org.

■ AUTHOR INFORMATION

Corresponding Author

yanyan.cao@usa.dupont.com

Notes

The authors declare no competing financial interest.

■ ACKNOWLEDGMENTS

The authors thank all the research supports on this project for their wonderful work. We thank our colleagues at the DuPont Corporate Center for Analytical Sciences, especially Joseph Galperin, Jing Li, Dennis Walls, Keith Warrington, Lei Zhang, Shekhar Subramoney, Wayne Brubaker, Christopher D. Chan, Rick Z. Li, Kathy Lloyd, Mike Guise, Jane Ramsey, and Pat Cotts, for material characterization. We thank Lee A. Silverman and our patent liaison, Karin Karel, for helpful discussions, and Peter Carcia for his advice about sputtered thin films. We are also grateful for the consistent support and guidance from Jeffrey A. Sternberg and Steve C. Freilich.

REFERENCES

(1) Green, M. A. *Photovoltaic Specialists Conference (PVSC)*, 2010 35th IEEE, Honolulu, HI, June 20−25, 2010; pp 000550−000555.
(2) Ramasamy, K.; Malik, M. A.; O'Brien, P. *Chem. Commun.* **2012**, *48*, 5703−5714.
(3) Katagiri, H. *Thin Solid Films* **2005**, *480−481*, 426−432.
(4) Haight, R.; Barkhouse, A.; Gunawan, O.; Shin, B.; Copel, M.; Hopstaken, M.; Mitzi, D. B. *Appl. Phys. Lett.* **2011**, *98*, 253502/1−253502/3.
(5) Seol, J.-S.; Lee, S.-Y.; Lee, J.-C.; Nam, H.-D.; Kim, K.-H. *Sol. Energy Mater. Sol. Cells* **2003**, *75*, 155−162.
(6) Katagiri, H.; Jimbo, K.; Maw, W. S.; Oishi, K.; Yamazaki, M.; Araki, H.; Takeuchi, A. *Thin Solid Films* **2009**, *517*, 2455−2460.
(7) Wang, K.; Gunawan, O.; Todorov, T.; Shin, B.; Chey, S. J.; Bojarczuk, N. A.; Mitzi, D.; Guha, S. *Appl. Phys. Lett.* **2010**, *97*, 143508/1−143508/3.
(8) Redinger, A.; Berg, D. M.; Dale, P. J.; Siebentritt, S. *J. Am. Chem. Soc.* **2011**, *133*, 3320−3323.
(9) Katagiri, H.; Sasaguchi, N.; Hando, S.; Hoshino, S.; Ohashi, J.; Yokota, T. *Sol. Energy Mater. Sol. Cells* **1997**, *49*, 407−414.
(10) Friedlmeier, T. A. M. *Fortschr.-Ber. VDI, Reihe 9* **2001**, *340* (i−xiii), 1−108.
(11) Repins, I.; Beall, C.; Vora, N.; DeHart, C.; Kuciauskas, D.; Dippo, P.; To, B.; Mann, J.; Hsu, W.-C.; Goodrich, A.; Noufi, R. *Sol. Energy Mater. Sol. Cells* **2012**, *101*, 154−159.
(12) Chawla, V.; Clemens, B. *Photovoltaic Specialists Conference (PVSC)*, 2010 35th IEEE, Honolulu, HI, June 20−25, 2010; pp 001902-001905.
(13) Moholkar, A. V.; Shinde, S. S.; Babar, A. R.; Sim, K.-U.; Lee, H. K.; Rajpure, K. Y.; Patil, P. S.; Bhosale, C. H.; Kim, J. H. *J. Alloys Compd.* **2011**, *509*, 7439−7446.
(14) Scragg, J. J.; Berg, D. M.; Dale, P. J. *J. Electroanal. Chem.* **2010**, *646*, 52−59.
(15) Tanaka, K.; Fukui, Y.; Moritake, N.; Uchiki, H. *Sol. Energy Mater. Sol. Cells* **2011**, *95*, 838−842.
(16) Kishore Kumar, Y. B.; Suresh Babu, G.; Uday Bhaskar, P.; Sundara Raja, V. *Solar Energy Mater. Solar Cells* **2009**, *93*, 1230−1237.
(17) Kassim, A.; Tan, W.; Abdullah, A. H.; Nagalingam, S.; Min, H. S. *Maced. J. Chem. Chem. Eng.* **2010**, *29*, 97−103.
(18) Riha, S. C.; Parkinson, B. A.; Prieto, A. L. *J. Am. Chem. Soc.* **2009**, *131*, 12054−12055.
(19) Guo, Q.; Hillhouse, H. W.; Agrawal, R. *J. Am. Chem. Soc.* **2009**, *131*, 11672−11673.
(20) Steinhagen, C.; Panthani, M. G.; Akhavan, V.; Goodfellow, B.; Koo, B.; Korgel, B. A. *J. Am. Chem. Soc.* **2009**, *131*, 12554−12555.
(21) Shavel, A.; Arbiol, J.; Cabot, A. *J. Am. Chem. Soc.* **2010**, *132*, 4514−4515.
(22) Guo, Q.; Ford, G. M.; Yang, W.-C.; Walker, B. C.; Stach, E. A.; Hillhouse, H. W.; Agrawal, R. *J. Am. Chem. Soc.* **2010**, *132*, 17384−17386.
(23) Katagiri, H.; Jimbo, K.; Tahara, M.; Araki, H.; Oishi, K. *Mater. Res. Soc. Symp. Proc.* **2009**, 1165.
(24) Todorov, T. K.; Reuter, K. B.; Mitzi, D. B. *Adv. Mater. (Weinheim, Ger.)* **2010**, *22*, E156−E159.
(25) Barkhouse, D. A. R.; Gunawan, O.; Gokmen, T.; Todorov, T. K.; Mitzi, D. B. *Prog. Photovoltaics: Res. Appl.* **2012**, *20*, 6−11.
(26) Cao, Y. (E.I. du Pont de Nemours and Company, USA). WO2011065994, 2011.
(27) Jiang, C.; Lee, J.-S.; Talapin, D. V. *J. Am. Chem. Soc.* **2012**, *134*, 5010−5013.
(28) Joo, J.; Na, H. B.; Yu, T.; Yu, J. H.; Kim, Y. W.; Wu, F.; Zhang, J. Z.; Hyeon, T. *J. Am. Chem. Soc.* **2003**, *125*, 11100−11105.
(29) Shafarman, W. N.; Stolt, L. In *Handbook of Photovoltaic Science and Engineering*; Luque, A., Hegedus, S., Eds.; John Wiley & Sons: New York, 2003; pp 568−616.
(30) Altosaar, M.; Raudoja, J.; Timmo, K.; Danilson, M.; Grossberg, M.; Krustok, J.; Mellikov, E. *Phys. Status Solidi A* **2008**, *205*, 167−170.
(31) Zoppi, G.; Forbes, I.; Miles, R. W.; Dale, P. J.; Scragg, J. J.; Peter, L. M. *Prog. Photovoltaics* **2009**, *17*, 315−319.
(32) Rosenfeld, H. D.; Ionkin, A. S.; Cao, Y.; Johnson, L. K.; Lu, M.; Radu, D.; Caspar, J. V.; Guise, W. E.; Galperin, J.; Marshall, W. J. *X-Ray Spectrom.* **2012**, submitted.
(33) Mitzi, D. B.; Gunawan, O.; Todorov, T. K.; Wang, K.; Guha, S. *Sol. Energy Mater. Sol. Cells* **2011**, *95*, 1421−1436.
(34) Niemegeers, A.; Burgelman, M. *J. Appl. Phys.* **1997**, *81*, 2881−2886.